Journal of Non-Crystalline Solids 358 (2012) 1374–1379

Contents lists available at SciVerse ScienceDirect

Journal of Non-Crystalline Solids

journal homepage: www.elsevier.com/ locate/ jnoncrysol

AES and FTIR characterization of sol–gel alumina films

Daniela C.L. Vasconcelos, Eduardo H.M. Nunes, Wander L. Vasconcelos *

Federal University of Minas Gerais, Dept. of Metallurgical and Materials Engineering Laboratory of Ceramic Materials, Avenida Presidente Antônio Carlos, 6627, sala 2230, Pampulha, Campus UFMG, Escola de Engenharia, bloco 2, CEP 31270-901, Belo Horizonte, MG, Brazil

ARTICLE INFO

Article history:
Received 28 December 2011
Received in revised form 12 March 2012
Available online 5 April 2012

Keywords:
Sol–gel;
Alumina films;
Dip-coating;
FTIR;
Auger electron spectroscopy

ABSTRACT

In this work we obtained sol–gel alumina coatings on AISI 304 stainless steel substrates. Alumina sols were prepared by using aluminum isopropoxide (AI) as precursor, acetic acid (HOAc) as catalyst, ethanol (C_2H_5OH) or isopropanol (C_3H_8O) as solvent, and water. The as-prepared solutions were deposited on stainless steel substrates by means of the dip-coating technique. The obtained composites were characterized by Fourier transform infrared spectroscopy (FTIR) and Auger electron spectroscopy (AES). We observed that the concentration of Al – O type bonds in the obtained alumina coatings depends on the solvent type used, temperature and peptization state of the sol, withdrawal speed, and number of dipping cycles. AES experiments showed that the interface formed between the alumina coating and substrate surface is in general formed by several layers of different chemical compositions.

1. Introduction

Coating composites, or surface engineered materials, are designed specifically to improve properties such as optical, electrical, tribological, chemical, and biological, among others [1]. The sol–gel process is very attractive in coating technology because coatings obtained by this method are usually homogeneous at a molecular level, and have tailored thicknesses and porosities [2–4]. In addition, substrates with any shape and size can be coated by sol–gel.

In order to improve the corrosion resistance of metals by applying coatings, various sol–gel oxide films have been studied. Using tetraethylorthosilane as starting material, Vasconcelos et al. [5] obtained sol–gel silica/304 stainless steel composites with higher corrosion resistance in a 1 N H_2SO_4 and 3.5% NaCl medium. Based on Rutherford Backscattering Spectroscopy data, the authors concluded that the intermediate layer formed between the silica film and steel substrate is responsible for improving the stainless steel corrosion resistance. Ruhi et al. [6] reported an increase in chemical resistance against mine water of steel sheets coated with sol–gel alumina films. Chou et al. [7] investigated the corrosion resistance of organic–inorganic sol–gel hybrid coatings on 304 and 316L stainless steel substrates. Conde [8] studied protective properties of sol–gel coatings deposited on galvannealed and galvanized steel samples. They noticed remarkable differences in coating properties depending on the substrate type and sintering temperature.

The protection of stainless steel against acid corrosion by polymer coatings has also been proposed [9,10]. However, these materials cannot be exposed to high temperatures or aggressive environments [11,12]. According to Vasconcelos [13], metallic coatings present the same constraints. In this work we prepared sol–gel alumina coatings on AISI 304 stainless steel substrates. The obtained composites were characterized by Fourier transform infrared (FTIR) and Auger electron (AES) spectroscopies.

2. Experimental

In this study, AISI 304 stainless steel plates of 0.5 mm thickness were cut into pieces of 3.0 cm × 3.0 cm. The chemical composition of the stainless steel used is the following: Cr (18.3 wt.%), Ni (8.2 wt.%), Mn (1.3 wt.%), Cu (0.08 wt.%), V (0.05 wt.%), Al (0.02 wt.%), Ti (0.02 wt.%). Prior to coating, the substrates were polished until 600 mesh, washed with detergent, deionized water, and degreased with acetone. Finally, they were placed in an ultrasonic bath with acetone and dried under hot air.

Alumina sols were prepared by using aluminum isopropoxide (AI) as precursor, acetic acid (HOAc) as catalyst, ethanol (C_2H_5OH) or isopropanol (C_3H_8O) as solvent, and water. We used the following molar ratios: water:precursor = 15, 20, 30, and 50; solvent:precursor = 5; solvent:catalyst = 2.5. Sols were obtained at room temperature and 70 °C, in both peptized and unpeptized states. The as-prepared solutions were deposited on stainless steel substrates by means of the dip-coating technique, using withdrawal speeds of 90 mm/min, 180 mm/min, and 400 mm/min. The number of dipping cycles ranged from 1 to 3. Between the successive dipping cycles the coated substrates were heat treated at 80 °C, 100 °C, or 600 °C for 30 min in an open to air oven.

FTIR spectra were recorded using a Perkin Elmer Paragon 1000 and employing the specular reflectance (SR) technique with an incidence angle of 45°. Data were collected with a 4 cm^{-1} resolution and

* Corresponding author.
E-mail address: wlv@demet.ufmg.br (W.L. Vasconcelos).

0022-3093
doi:10.1016/j.jnoncrysol.2012.03.017

64 scans were accumulated for each spectrum. The effect of changing synthesis parameters on the obtained infrared spectra was evaluated by using the absorption band at about 3430 cm^{-1} as reference. In these analyses we considered the spectral range from 1370 cm^{-1} to 450 cm^{-1} because absorption bands related to Al–O type bonds are present in this region. The depth composition profile of the processed composites was obtained by the joint use of AES and sputter depth profiling. In these analyses we took into consideration the following chemical elements: Fe, Cr, Ni, Al, and O. AES tests were performed within an experimental error of about 5%. It is worth mentioning that O was only detected in trace amounts, especially in the outermost layers of the composites. We believe that this drawback arises from the fact that AES requires the use of standards with compositions as close as possible to those of the analyzed materials in order to quantify the measurements. Furthermore, in AES analyses chemical binding effects may influence the tests [14]. For sake of clarity we decided to not show the results related to oxygen in this work.

3. Results

3.1. FTIR

The typical FTIR spectrum of an AISI 304 stainless steel substrate coated with a sol–gel alumina film and heat treated at 100 °C is shown in Fig. 1. The broad absorption band around 3430 cm^{-1} is due to products derived from aluminum alkoxide hydrolysis and hydroxyl groups present on the surface of pseudo-boehmite and boehmite [15–17]. The bands at 3020 cm^{-1} and 2930 cm^{-1} are ascribed to asymmetric and symmetric stretching vibrations of CH_3 and CH_2 groups, respectively [18]. The absorption peak at 1484 cm^{-1} is assigned to the bending mode of CH_2 groups. The bands at 1638 cm^{-1} and 1445 cm^{-1} are respectively due to the asymmetric $\nu_{as}(COO)$ and symmetric $\nu_s(COO)$ stretching vibrations. These two absorption bands are related to the use of acetic acid in syntheses [19]. Superimposed onto the band at 1638 cm^{-1}, a component at 1630 cm^{-1}, ascribed to the presence of physisorbed water on films surface, is also observed [16,20]. The stretching vibration of the Al═O bond is present at 1350 cm^{-1} [21]. The bands around 1000 cm^{-1} are related to stretching modes of AlO_4 tetrahedra, whereas those near 680 cm^{-1} and 570 cm^{-1} are assigned to stretching vibrations of AlO_6 octahedra [18,22].

Fig. 2 shows infrared spectra of samples obtained by using isopropanol or ethanol as solvent in syntheses. The sample obtained using ethanol showed a higher absorbance in the spectral region assigned to Al–O type bonds. This indicates that films processed using ethanol as solvent presented a greater concentration of Al–O bonds in their structures. As shown in Fig. 3, the sol temperature also affects the concentration of Al–O bonds in films. We observed that the coating

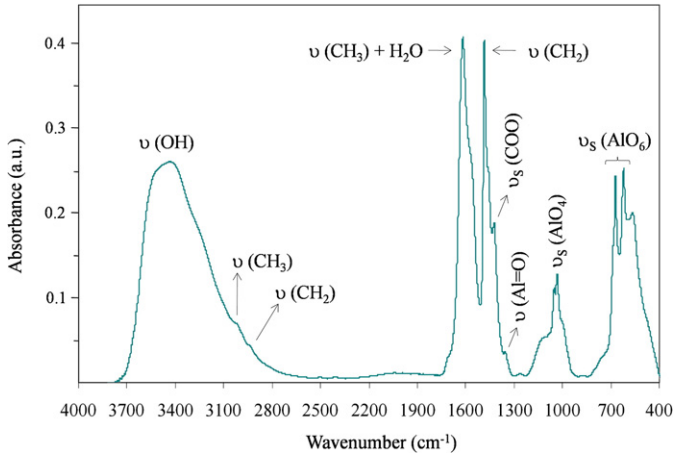

Fig. 1. Typical FTIR spectrum of an AISI 304 stainless steel substrate coated with a sol–gel alumina film and heat treated at 100 °C.

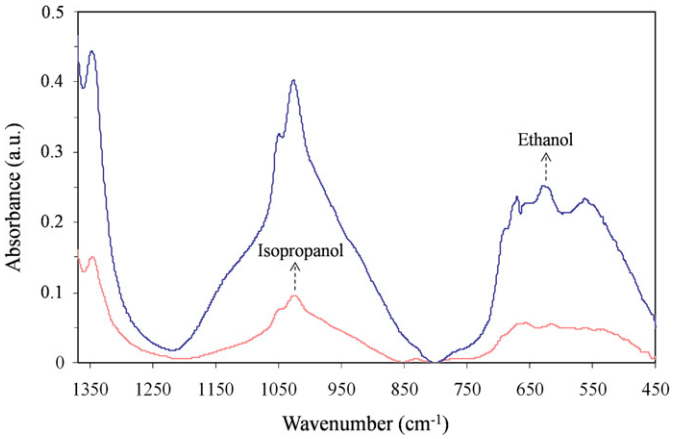

Fig. 2. FTIR spectra of samples obtained using ethanol and isopropanol as solvents in synthesis. Samples obtained by fixing the H_2O:Al molar ratio at 50.

obtained using the alumina sol at room temperature showed a greater amount of Al–O type bonds in its structure than that processed using the sol at 70 °C.

Alumina sols can be obtained in peptized and unpeptized states. The peptization process can be defined as the redispersion of a coagulated sol. Thus, during the peptization process the aggregates formed in the condensation step are destroyed, decreasing the aggregation state of particles into a large extent [23]. As shown in Fig. 4, the film obtained from a peptized sol presented a higher density of Al–O type bonds.

Fig. 5 shows the infrared spectra of AISI 304 stainless steel substrates coated with alumina films withdrawn at 90 mm/min, 180 mm/min, and 400 mm/min. We observed that the greater the withdrawal speed, the higher the presence of Al–O bonds in the film. Fig. 6 shows the infrared spectra of alumina films obtained using distinct numbers of dipping cycles. We observed that the greater the number of dipping cycles, the higher the presence of Al–O bonds in the coating. Based on these results we decided to carry out the AES tests in composites prepared using ethanol as solvent, the alumina sol at room temperature and in the peptized state, a withdrawal speed of 400 mm/min, and three dipping cycles.

3.2. AES

Fig. 7 shows the depth composition profile and a schematic representation of AISI 304 stainless steel substrates used in this work. We observed the presence of chemical elements inherent to the analyzed steel: Fe, Ni, and Cr. One notices that aluminum was not detected.

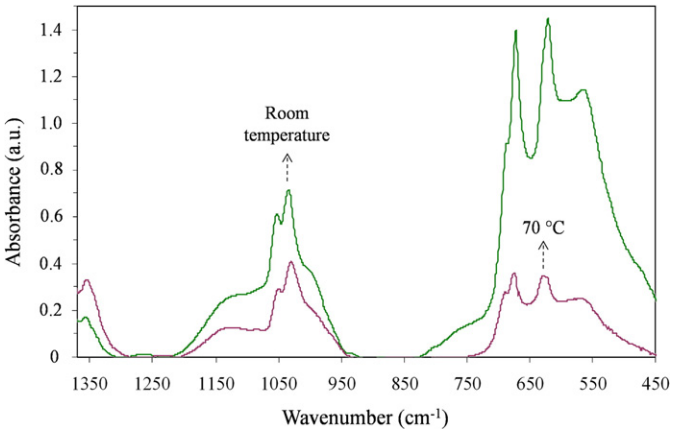

Fig. 3. FTIR spectra of samples obtained using the alumina sol at room temperature and 70 °C. Samples obtained by fixing the H_2O:Al molar ratio at 20.

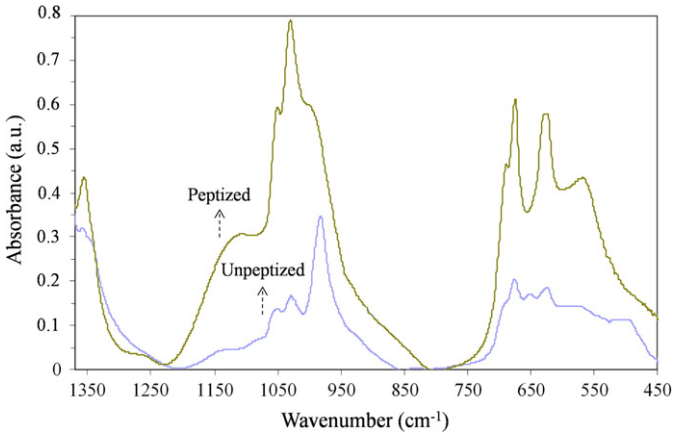

Fig. 4. FTIR spectra of samples obtained using peptized and unpeptized alumina sols. Films obtained by fixing the H_2O:AI molar ratio at 15.

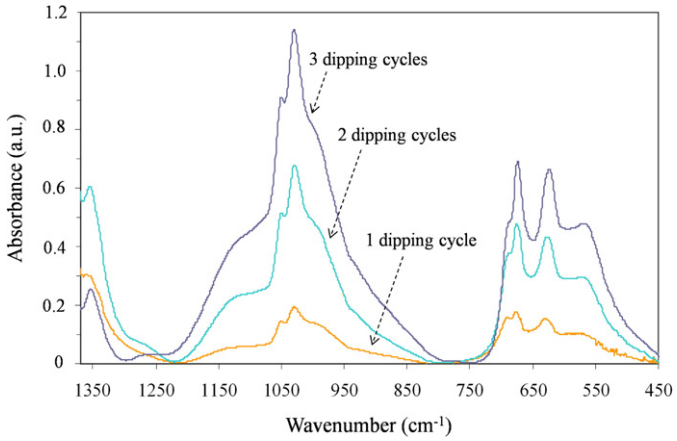

Fig. 6. FTIR spectra of AISI 304 steel substrates coated using distinct dipping cycles. Films obtained by fixing the H_2O:AI molar ratio at 30.

Fig. 8 (a) shows the depth composition profile of stainless steel/sol–gel alumina composite, whose alumina film was prepared by fixing the molar ratios of H_2O:AI and HOAc:AI at 30 and 0.5, respectively. One observes the presence of only Al at depths below about 90 nm. The first trace amounts of Fe are only observed at depths from 90 nm to 98 nm, whereas Cr and Ni are detected at depths above 98 nm and 125 nm, respectively. As schematically represented in Fig. 8 (b), this result indicates that Fe, and in a less extent Ni and Cr, diffused into the alumina layer.

As shown in Fig. 9, when this composite was heat treated at 600 °C the alumina coating presented a decrease in thickness of about 50%. In addition, the interface exhibited a change in structure after heating: the Al–Fe layer showed an increase in thickness from about 8 nm to 35 nm, the Al–Fe–Cr–Ni layer disappeared, and three new layers were created (Al–Fe–Cr, Fe–Cr, and Fe–Cr–Ni). This behavior suggests that the aforementioned diffusion of Fe, Cr, and Ni is enhanced by the heat treatment at 600 °C.

The depth composition profile of the composite obtained by changing the H_2O:AI molar ratio from 30 to 60 is presented in Fig. 10. In this synthesis the obtained alumina sol had a low concentration of AI, which resulted in a thinner alumina coating of about 28 nm thickness. Thereafter we observed an Al–Fe layer until a depth of 35 nm, an Al–Fe–Cr layer until 42 nm, and an Al–Fe–Cr–Ni layer until 70 nm. We noticed that differently from the composite prepared using a H_2O:AI molar ratio of 30, this sample showed the Al–Fe–Cr–Ni layer in its structure even when heat treated at a temperature as low as 80 °C.

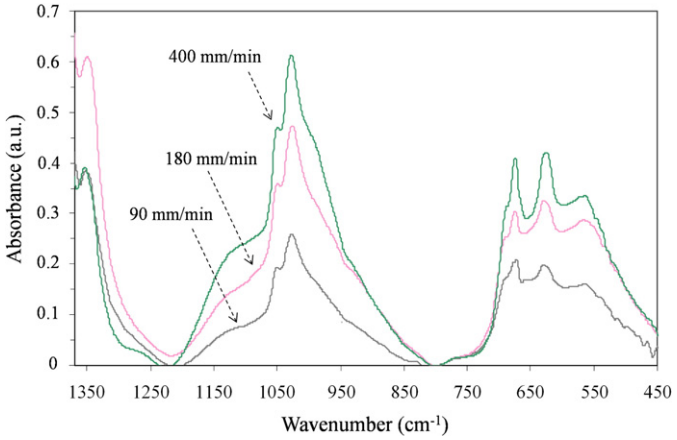

Fig. 5. FTIR spectra of AISI 304 stainless steel substrates coated with alumina films withdrawn at 90 mm/min, 180 mm/min, and 400 mm/min. Films obtained by fixing the H_2O:AI molar ratio at 30.

The composite whose depth composition profile is shown in Fig. 11 was obtained by using a H_2O:AI molar ratio of 60, and a heat treatment temperature of 600 °C. We observed the presence of the Al–Fe layer until a depth of about 30 nm. Velez and Quinson [15] noticed that Fe diffusion into the alumina coating is more pronounced the thinner the film. The Al–Fe–Cr layer is observed until depths of 58 nm, the Fe–Cr layer until 63 nm, and the Fe–Cr–Ni layer until about 80 nm.

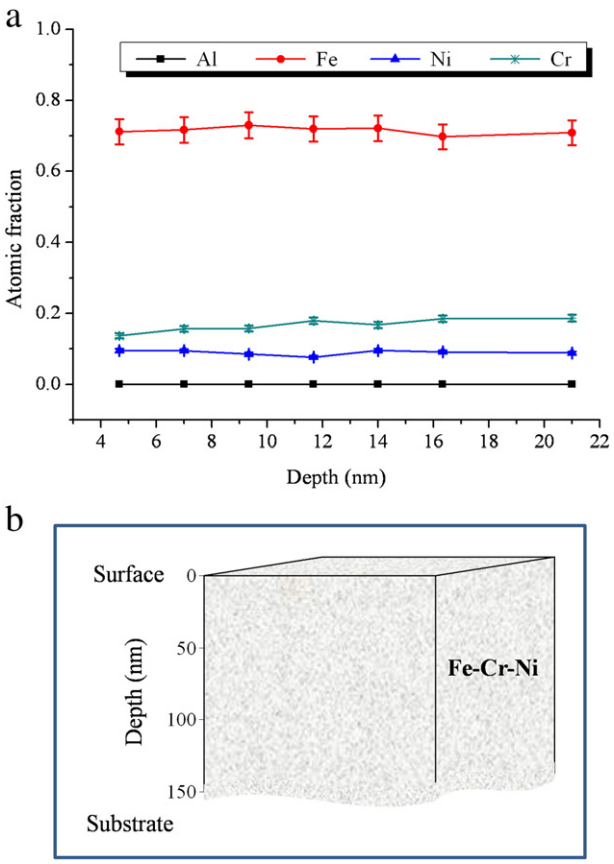

Fig. 7. (a) Depth composition profile and (b) schematic representation of the AISI 304 stainless steel. The straight lines connecting the data points are used only as guide to the eyes.

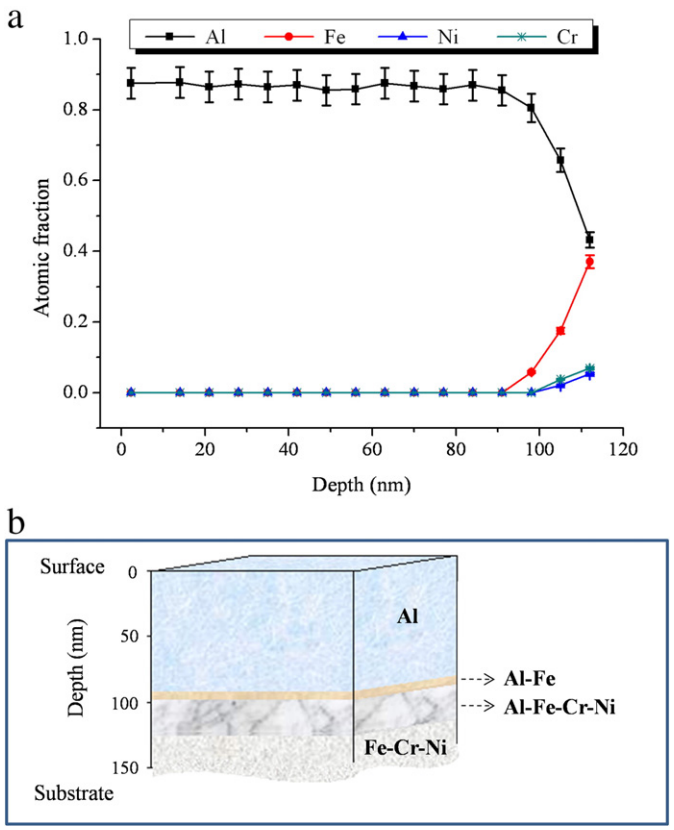

Fig. 8. (a) Depth composition profile and (b) schematic representation of AISI 304 stainless steel coated with sol–gel alumina film and heat treated at 80 °C (H_2O:Al = 30, and HOAc:Al = 0.5). The straight lines connecting the data points are used only as guide to the eyes.

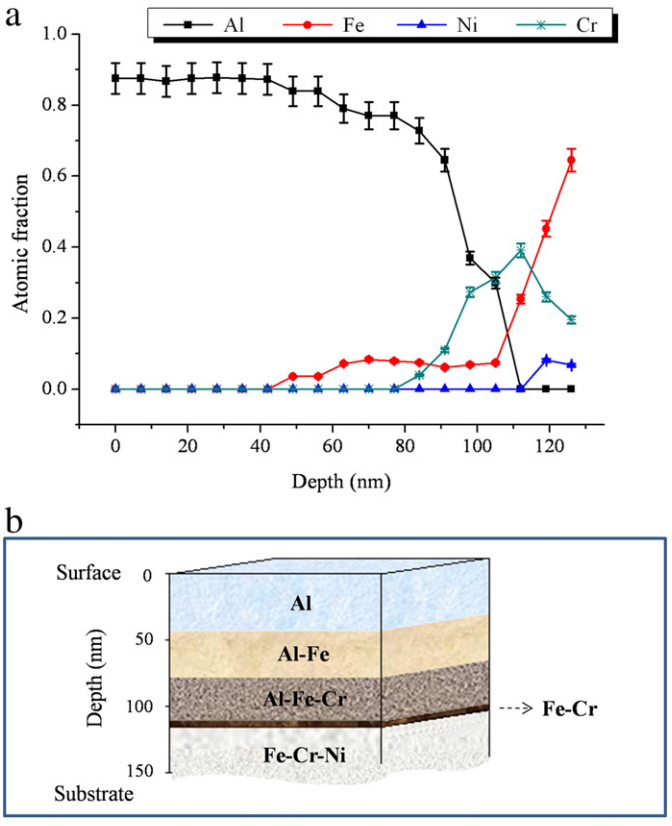

Fig. 9. (a) Depth composition profile and (b) schematic representation of AISI 304 stainless steel coated with sol–gel alumina film and heat treated at 600 °C (H_2O:Al = 30, and HOAc:Al = 0.5). The straight lines connecting the data points are used only as guide to the eyes.

4. Discussion

It is well established that in the dip-coating process the film thickness (h) can be expressed by the Landau–Levich equation [24–27]:

$$h = 0.94\frac{(\eta\cdot U)^{2/3}}{\gamma_{LV}^{1/6}(\rho\cdot g)^{1/2}}, \quad (1)$$

where U represents the substrate withdrawal speed, η and ρ the viscosity and density of the sol, γ_{LV} the liquid–vapor surface tension, and g the gravity. From Eq. (1) one notices that the greater the withdrawal speed, the thicker the sol–gel coating. We observed that the greater the withdrawal speed, the higher the presence of Al – O bonds in the film (see Fig. 5). This behavior could be related to the formation of thicker films as the withdrawal speed was increased from 90 mm/min to 400 mm/min. It is stated in the literature that the intensity of a given FTIR band is related to the concentration of absorbent species in the sample [28]. Thus, one could expect that the thicker the alumina film, the more intense the infrared bands ascribed to Al – O type bonds.

Ung et al. [29] prepared homogeneous films of Au–SiO_2 particles on glassy substrates. Film thicknesses were controlled by the number of dipping cycles and evaluated by Atomic Force Microscopy. They reported that the greater the number of dipping cycles, the thicker the obtained film. We observed that increasing the number of dipping cycles from 1 to 3 leads to films whose FTIR spectra are more intense in the spectral region related to Al – O type bonds (see Fig. 6). We believe that this behavior could be related to the formation of thicker films as the number of dipping cycles was increased.

Brinker and Scherer [26,30] reported that the relative rates of condensation and evaporation of a given sol will depend on its aggregation degree. The authors reported that the more dispersed the particles in the sol, the lower the relative evaporation rate and the thicker the film. FTIR tests revealed that the film obtained from a peptized sol presented a higher density of Al – O type bonds in its framework than that obtained from a non-peptized sol (see Fig. 4). We believe that this behavior could be related to the preparation of thicker films when peptized sols are used in syntheses.

One observes from Eq. (1) that the thickness of a dip-coated film is related to the sol viscosity; the higher the sol viscosity, the thicker the film. According to Zelinski and Uhlmann [31], the gelation behavior of colloidal and polymeric gels depends on processing variables including solvent type and concentration, catalyst concentration, and sol temperature. Thus, one would expect that coatings obtained using distinct solvent types and sol temperatures could present different thicknesses, since these parameters influence the sol viscosity [26,30]. We observed that coatings prepared using the sol at room temperature and ethanol as solvent exhibited greater thicknesses than those obtained using the sol at 70 °C and isopropanol as solvent (see Figs. 2 and 3). Another issue that must be taken into consideration is that the FTIR spectra were normalized using the broad absorption band at about 3430 cm^{-1} as reference. As mentioned before, this band is ascribed to products derived from aluminum alkoxide hydrolysis and hydroxyl groups present on the surface of pseudo-boehmite and boehmite [15–17]. It is well established that the precursor hydrolysis is related to the solvent type and sol temperature. Thus, the relative intensity of the infrared band at 3430 cm^{-1} will depend on these processing parameters.

The depth profile obtained by AES for AISI 304 stainless steel used in this study matches with the chemical composition of this material: Cr (18.3 wt.%), Ni (8.2 wt.%), and Al (0.02 wt.%) (see Fig. 7). AES tests

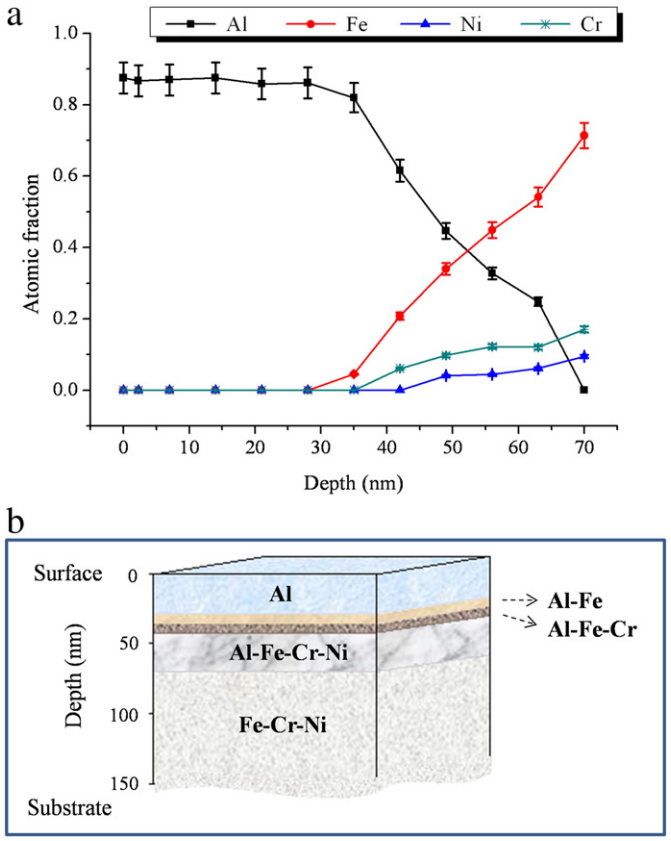

Fig. 10. (a) Depth composition profile and (b) schematic representation of AISI 304 stainless steel coated with sol–gel alumina film and heat treated at 80 °C (H_2O:Al = 60, and HOAc:Al = 0.5). The straight lines connecting the data points are used only as guide to the eyes.

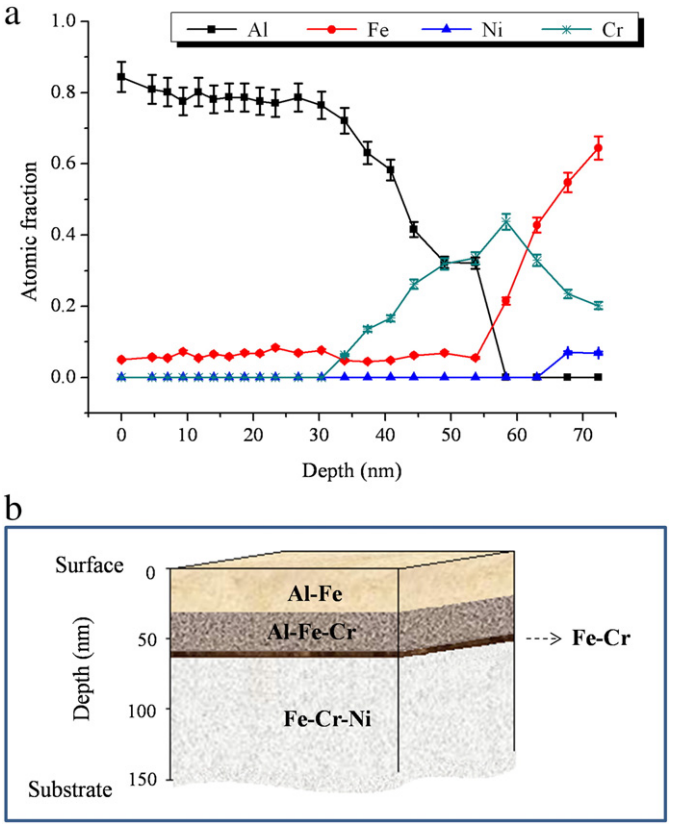

Fig. 11. (a) Depth composition profile and (b) schematic representation of AISI 304 stainless steel coated with sol–gel alumina film and heat treated at 600 °C (H_2O:Al = 60, and HOAc:Al = 0.5). The straight lines connecting the data points are used only as guide to the eyes.

revealed that the interface present between the alumina coating and substrate surface is in general formed by several layers of different chemical compositions. One observes by comparing Figs. 8 to 11 that increasing the heat treatment temperature of composites enhances the atomic diffusion of Fe, Cr, and Ni into the alumina layer. Hourmard et al. [32] investigated the surface physico-chemistry properties of stainless steel and the effects of a cold rolling treatment. They performed X-ray photoelectron spectroscopy analyses on rolled surfaces at different rates. The authors noticed an iron enrichment of the passive film during the cold rolling treatment, which seems to be related to a surface heating during the mechanical treatment. Thus, the mechanical treatment increased the stainless steel temperature, which in turn enhanced the diffusion of Fe towards the surface.

We observed that differently from the composite prepared using a H_2O:Al molar ratio of 30, the composite obtained using a H_2O:Al molar ratio of 60 showed the Al–Fe–Cr–Ni layer in its framework even when heat treated at a temperature as low as 80 °C (see Fig. 10). In addition, the composite obtained using a H_2O:Al molar ratio of 30 presented an alumina coating on its surface even when heat treated at 600 °C (see Fig. 9). AES tests revealed that samples obtained using the aforementioned molar ratio equal to 60 did not show an alumina coating on their surface after the heat treatment at 600 °C (see Fig. 11). We believe that this behavior could arise from the use of a more acidic alumina sol in the processing of this composite. This may have caused a significant chemical attack of the substrate surface.

5. Conclusions

FTIR tests revealed that the concentration of Al – O type bonds in the obtained alumina coatings depends on the solvent type used, temperature and peptization state of the sol, withdrawal speed, and number of dipping cycles. We believe that the observed variation on the concentration of Al – O type bonds in films could be related, in a large extent, to changes in their thicknesses. Another issue that must be taken into consideration is that the FTIR spectra were normalized using the band at about 3430 cm^{-1} as reference. Since this band is ascribed to products derived from aluminum alkoxide hydrolysis and hydroxyl groups present in samples framework, its intensity could depends on the synthesis parameters used in this work.

AES tests showed that the interface formed between the alumina coating and substrate surface is in general formed by several layers of different chemical compositions. The increase of the film heat treatment temperature enhanced the diffusion of Fe, Cr, and Ni into the alumina layer. We observed that the alumina coating thickness is related to the concentration of AI in the starting sol: the higher the alkoxide concentration, the thicker the coating. We also noticed that differently from the composite prepared using a H_2O:AI molar ratio of 30, the composite obtained using a H_2O:AI molar ratio of 60 showed the Al–Fe–Cr–Ni layer in its structure even when heat treated at a temperature as low as 80 °C. We believe that this behavior arises from the use of a more acidic alumina sol in the processing of this composite, since this may have caused a severe chemical attack of the substrate surface.

Acknowledgments

The authors thank the financial support from the Minas Gerais Research Agency (FAPEMIG) and Brazilian Research Agency (CNPq). We also thank prof. Dr. Manuel Houmard for his comments and suggestions about this work.

References

[1] S. Hogmark, S. Jacobson, M. Larsson, Wear 246 (2000) 20–33.
[2] L.L. Hench, W.L. Vasconcelos, Annu. Rev. Mater. Sci. 20 (1990) 269–298.
[3] C.J. Brinker, C.S. Ashley, R.A. Cairncross, K.S. Chen, A.J. Hurd, S.T. Reed, J. Samuel, P.R. Schunk, R.W. Schwartz, C.S. Scotto, in: K.H. Stern (Ed.), Metallurgical and Ceramic Protective Coatings, Chapman & Hall, London, 1996, pp. 112–120.
[4] H. Dislich, in: L.C. Klein (Ed.), Sol–gel Technology for Thin Films, Fibers, Performs, Electronics and Specialty Shapes, Noyes Publications, New Jersey, 1988, pp. 50–79.
[5] D.C.L. Vasconcelos, J.A.N. Carvalho, M. Mantel, W.L. Vasconcelos, J. Non-Cryst. Solids 273 (2000) 135–139.
[6] G. Ruhi, O.P. Modi, A.K. Jha, I.B. Singh, Indian J. Chem. Technol. 16 (2009) 216–220.
[7] T.P. Chou, C. Chandrasekaran, S. Limmer, C. Nguyen, Z. Cao, J. Mater. Sci. Lett. 21 (2002) 251–255.
[8] A. Conde, J. de Damborenea, A. Dúran, M. Menning, J. Sol-Gel Sci. Technol. 37 (2006) 79–85.
[9] G. Grundmeier, W. Schmidt, M. Stratmann, Electrochim. Acta 45 (2000) 2515–2533.
[10] S. de Souza, J.E.P. da Silva, S.I.C. de Torresi, M.L.A. Temperini, R.M. Torresi, Electrochem. Solid-State Lett. 4 (2001) B27–B30.
[11] H. Cao, R. Zhang, C.S. Sundar, J.-P. Yuan, Y. He, T.C. Sandreczki, Y.C. Jean, B. Nielsen, Macromolecular 31 (1998) 6627–6635.
[12] A. Miszczyk, K. Darowicki, Prog. Org. Coat. 46 (2003) 49–54.
[13] D.C.L. Vasconcelos, Non-oriented grain silicon steel/stainless steel composites coated with magnesia, alumina, silica and titania films prepared by sol–gel, PhD. Thesis, Federal University of Minas Gerais, 2003.
[14] K.K. Bourdelle, Nucl. Instrum. Methods Phys. Res. B66 (1992) 274–279.
[15] K. Velez, J.F. Quinson, J. Sol-Gel Sci. Technol. 19 (2000) 469–472.
[16] J.A. Wang, X. Bokhimi, A. Morales, O. Novaro, T. López, R. Gómez, J. Phys. Chem. B 103 (1999) 299–303.
[17] V. Jayaraman, T. Gnanasekaran, G. Periaswami, Mater. Lett. 30 (1997) 157–162.
[18] P. Padmaja, G.M. Anilkumar, P. Mukundan, G. Aruldhas, K.G.K. Warrier, Int. J. Inorg. Mater. 3 (2001) 693–698.
[19] R. Urlaub, U. Posset, R. Thull, J. Non-Cryst. Solids 265 (2000) 276–284.
[20] S.-C. Shen, W.K. Ng, Z.-Y. Zhong, Y.-C. Dong, L. Chia, R.B.H. Tan, J. Am. Ceram. Soc. 92 (2009) 1311–1316.
[21] A. Raveh, Z.K. Tsameret, E. Grossman, Surf. Coat. Technol. 88 (1996) 103–111.
[22] A.G. Alejandre, M.G. Cruz, M. Trombetta, G. Busca, J. Ramírez, Microporous Mesoporous Mater. 23 (1998) 265–275.
[23] H.Y. Lee, G.M. Kale, Int. J. Appl. Ceram. Technol. 5 (2008) 657–665.
[24] L.D. Landau, B.G. Levich, Acta Physicochim. URS 17 (1942) 42–54.
[25] I.M. Thomas, in: L.C. Klein (Ed.), Sol–gel Optics: Processing and Applications, Springer, Boston, 1994, pp. 141–158.
[26] C.J. Brinker, G.W. Scherer, in: C.J. Brinker, G.W. Scherer (Eds.), Sol–gel Science: The Physics and Chemistry of Sol–gel Processing, Academic Press Inc., San Diego, 1990, pp. 787–838.
[27] C.J. Brinker, A.J. Hurd, P.R. Schunk, G.C. Frye, C.S. Ashley, J. Non-Cryst. Solids 147–148 (1992) 424–436.
[28] D.A. Skoog, D.M. West, in: D.A. Skoog, D.M. West (Eds.), Principles of Instrumental Analysis, Saunders College, Philadelfia, 1980, pp. 209–254.
[29] T. Ung, L.M. Liz-Marzán, P. Mulvaney, J. Phys. Chem. B 105 (2001) 3441–3452.
[30] C.J. Brinker, G.W. Scherer, in: C.J. Brinker, G.W. Scherer (Eds.), Sol–gel Science: The Physics and Chemistry of Sol–gel Processing, Academic Press Inc., San Diego, 1990, pp. 97–228.
[31] B.J.J. Zelinski, D.R. Uhlmann, J. Phys. Chem. Solids 45 (1984) 1069–1090.
[32] M. Houmard, G. Berthomé, L. Boulangé, J.C. Joud, Corros. Sci. 49 (2007) 2602–2611.